Title
Metal-Organic Framework Additive in Electrolyte for Rechargeable Zinc-ion Battery

Author
An, Bowen

Publication Date
2021

Peer reviewed|Thesis/dissertation

UNIVERSITY OF CALIFORNIA

Los Angeles

Metal-Organic Framework Additive in Electrolyte for Rechargeable Zinc-ion Battery

A thesis submitted in partial satisfaction

of the requirements for the degree Master of Science

in Chemical Engineering

by

Bowen An

2021

ABSTARCT OF THE THESIS

Metal-Organic Framework Additive in Electrolyte

for Rechargeable Zinc-ion Battery

by

Bowen An

Master of Science in Chemical Engineering

University of California, Los Angeles, 2021

Professor Yunfeng Lu, Chair

Rechargeable aqueous zinc batteries have attracted large attention due to their high safety and low cost. During the charging process, however, the cycling life is limited by dendrite formation because the desolvation process of hexaaqua zinc cation complex $[Zn(H_2O)_6]^{2+}$ is incomplete and sluggish. Herein, two Zr-based metal-organic frameworks (MOFs) called UIO-66 and MOF-808 respectively, were used as additive into the electrolyte in order to improve the cycling life and accelerate the desolvation process. With the foundation of coin cell testing platform of Zn vs Zn symmetric battery, it can be clearly seen that the overpotential is decreased and the cycling life is prolonged. With the help of electrochemical impedance spectroscopy (EIS), it is proved that the desolvation process can be accelerated with the help of Zr-based MOFs additive.

The thesis of Bowen An is approved.

Yuzhang Li

Philippe Sautet

Yunfeng Lu, Committee Chair

University of California, Los Angeles

2021

Table of Contents

List of Figures

Acknowledgements

I would like to thank Prof. Yunfeng Lu and his whole lab members. I am still very grateful that Prof. Yunfeng Lu offered me this opportunity to study in UCLA, make friends with people here and experience life in Los Angeles, California. Additionally, thanks to Dr. Li Shen's detailed instruction.

I also would like to thank Prof. Yuzhang Li and Prof. Philippe Sautet for being in my committee and reviewing this work. Thank you for your suggestions about analyzing the data and writing the thesis.

Finally, I must send my gratitude for my family. Thank you for always understanding and supporting me.

1 Introduction

Huge release of gases including CO_2, NO and SO_2 into the atmosphere results in global warming and environmental issues, whereas the consumption of fossil fuels is still rapidly increasing. Compared with fossil fuels, wind and solar energy are environmental-friendly and unlimitedly free, making them extremely promising alternative candidates for renewable energy resources. However, these resources are not constantly accessible, thus energy storage is vital, where battery systems play an important role[1,2].

In 2018, 28.4% (almost one third) of total greenhouse gas emissions in USA generates from the transportation, which is an extremely huge portion[3]. Thus, traditional gasoline-powered vehicles highly need replacing by Battery Electric Vehicles (BEVs) where more renewable clean energy can be utilized. By March 31st, 2019, over 1.18 million electric vehicles had occupied the market, and there is a 10% increase from the first quarter of 2018 to 2019[4]. However, the BEVs only dominate 1.8% in the market, which is far from popularity[5]. Even though California government has decided to prohibit sales of new gasoline-powered vehicles from 2035, the high cost, small range and slow "refueling" rate of BEVs are still huge challenges[6]. It is the battery pack that is responsible for the most significant cost for BEVs, thus the cost per kilowatt hour ($/kWh) needs decreasing, which will make the BEVs affordable for the public. According to Bloomberg NEF, the cost of an entire battery pack has decreased from $1,160/kWh in 2010 to $577/kWh in 2014 and $156/kWh in 2019[4]. This is a huge improvement, however, the target of battery packs cost should be below $125/kWh to compete with traditional gasoline-powered vehicles[7].

Since its introduction by Sony in 1991, Lithium-ion batteries (LIBs) have dominated the market for high-capacity applications, especially in limited spaces including the battery pack for BEVs[8]. In the past, Nickel-Metal Hydride (NiMH) batteries were used in Hybrid-Electric Vehicles

(HEVs), but NiMH batteries only delivered 60 to 120 Wh/kg and 300 to 500 cycles above 80% of rated capacity[9]. Compared with other rechargeable batteries, LIBs have amazing cycling life, thus they revolutionized our daily life through driving various portable electronics including notebook computers, cameras, and smart phones, and three researchers including John Goodenough, Stanley Whittingham, and Akira Yoshino were awarded the 2019 Nobel Prize in Chemistry because of their contributions for the development of lithium batteries[10,11]. However, lithium resource is not that abundant, and LIBs have small capacity, causing its high cost and limiting its application in large-scale devices including BEVs[12,13]. Thus, increasing the energy density of a battery cell is important. Additionally, the cost density ($/kWh) might hugely decrease as well because less raw materials are needed for a certain required energy.

Graphite anode (372 mAh/g) are the standard anode material for LIBs, and researchers have tried to use silicon (3,365 mAh/g in theory)[14] or pure lithium metal (3,860 mAh/g in theory) as the alternatives[15]. However, the volume of silicon anodes expands 300% during charging, which degrades rapidly and limits the cycling life of battery. Therefore, hybrid carbon-silicon structures including core−shell tubes, nanowires, and hollow and porous spheres are given huge attention due to their ability to allow volume expansion on the micro scale instead of severely increasing the bulk electrode volume during cycling.

Wang, J. et. al made the silicon nanoparticles coated with a dense silicon which is resistant from a pressure of over 100 MPa, making the electrode less vulnerable during the calendaring process. In addition, graphene cage was also coated to limit the expansion of silicon cage. The capacity can reach 1388 mAh/g and could maintain 300 cycles at a high rate of 0.5C[14]. Nanowires are also attractive since they allow the expansion perpendicular to the axis of the wires. Chan et. al synthesized silicon nanowires which exhibited a capacity of over 2100 mAh/g for 20 cycles at

0.5C[16], and Fan et al. made silicon nanowires with a capacity of 2400 mAh/g over 200 cycles with graphene coated on the current collector to prevent parasitic silicon layer forming[17]. However, silicon shell structures or nanowires cost much during the manufacture, and their cycling life is still too short. Thus, their commercialization is still not feasible.

Anode material can also use pure lithium metal with extremely high capacity. However, lithium dendrite grows during the charging step, which can decrease the stability and even cause short circuit due to piercing the separator. Wang, H. et al. used wrinkled graphene cage (WGC) which helps to suppress volume fluctuation and dendrite growth during cycling, and it generates a capacity of 2785 mAh/g and an average columbic efficiency of 98% when applied with the 10 mAh/cm^2 current rate[15]. Salvatierra et al. used lithiated multiwall carbon nanotubes to control diffusion and the growth of lithium dendrites by regulating current densities, which makes the columbic efficiency near 99.9% for 450 cycles[18].

These results are promising, but their manufacturing cost are still quite high for a feasible application in automotive market. Additionally, the cycling stability of lithium metals is always a limitation. What's worse, LIBs use toxic and flammable organic electrolytes and the safety problem, such as the explosion of Samsung smart phones, is always a more dangerous threat which generates public concerns[19-21]. Those disadvantages are unavoidable, thus it is also essential to develop new battery systems as the alternative of LIBs.

Researchers are sparing no effort to study metal-based batteries with larger capacity using safe and cheap aqueous electrolytes. Up to now, there have been various rechargeable aqueous metal-ion batteries being developed and may dominate the energy storage system[22-24]. Zinc-ion batteries (ZIBs) are one of these candidates, and it is considerably focused and expected in large-scale energy storage systems in the future[25]. Here are the following reasons[26-29]: (1) Zn is more

abundant, which makes it much cheaper than lithium; (2) ZIB is not sensitive to moisture and air, thus inert environment is not required for assembly, which dramatically reduces expenses; (3) Zn metal can directly be the anode in aqueous system while other metals (lithium, magnesium, calcium, and aluminum) cannot. Zn is not quite reactive to water, and its electrodeposition is relatively reversible; (4) Zn metal owns high theoretical volumetric capacity (5855 mAh/cm^3) and gravimetric capacity (820 mAh/g); (5) Zn metal and its salts are environmentally friendly; (6) Zn oxidation/reduction potential of vs. the standard hydrogen electrode is -0.76 V, indicating a possible high open voltage when coupled with a cathode. Such advantages have made ZIBs attractive in recent years.

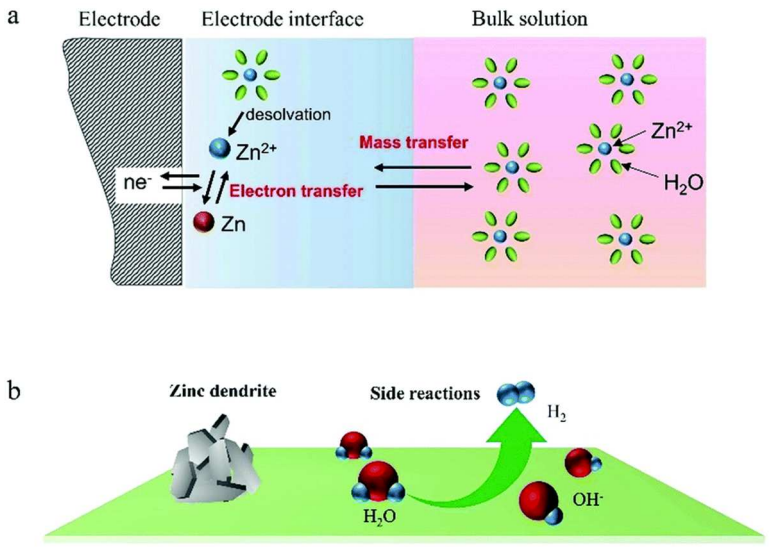

Figure 1. Ideal charge mechanism and real mechanism of aqueous zinc ion batteries from Ref.25

However, electrodeposition of Zn is likely to form non-uniform dendrite. In addition, the severe passivation caused by water would deteriorate this problem[25,30]. As it is shown in Figure.1, During the ideal charging process, hexaaqua zinc cation complex $[Zn(H_2O)_6]^{2+}$ shall desolvate firstly and generate a bare zinc cation Zn^{2+}. Next, this bare Zn^{2+} shall diffuse to the electrode and

reduce to Zn metal. However, water has strong interaction with Zn^{2+}, causing the desolvation process sluggish and incomplete. Thus parasitic water might electro-decompose near the electrode interface, releasing H_2, leaving OH^- reacting with Zn^{2+} and forming $Zn(OH)_2$ and ZnO passivation layer. The micro-environment around the electrode fluctuates and make zinc electrodeposition have preferential direction, which might exacerbate dendrite[31,32]. Thus, improving the desolvation process is the key of improving the zinc electrode reversibility.

General ideas for a reversible Zn electrode include complex structure engineering and interfacial engineering. Complex structure engineering, aimed at alleviating water splitting, modifies the complex structure by replacing water with electrolyte additive. $[Zn(H_2O)_6]^{2+}$ occupies a high ratio in the electrolyte because $ZnSO_4$ has strong ionic bond and more water solvent is required to break all those bonds to completely dissolve $ZnSO_4$. The result is that the concentration of saturated $ZnSO_4$ electrolyte is only 3.3M, and $[Zn(H_2O)_6]^{2+}$ is still the dominate species. However, Wang et al. used ionic liquid as the solute, which has weak ionic bond and requires less solvent for solvation[33]. That is how high concentrated ("water-in-salt") electrolytes were created, in which most Zn^{2+} are closely coordinated with bis (tri-fluoromethanesulfonyl) imide ($TFSI^-$) in pairs and their derived interphase would drive uniform Zn deposition. However, the price of ionic liquid is quite high, which is disadvantageous in commercial application.

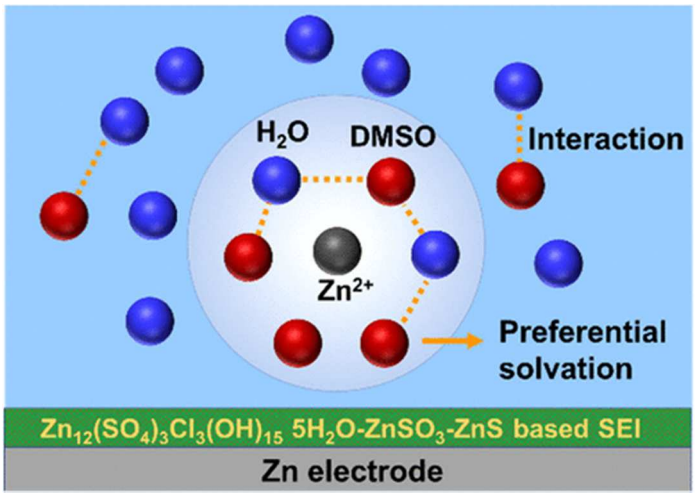

Figure 2. The effect of DMSO additive into electrolyte from Ref.34

Wang et al. used another method by adding Dimethyl sulfoxide (DMSO) inside the electrolyte[34], as it is shown in Figure 2. Since DMSO has larger Gutmann doner number (30) than that of water (18), Zn^{2+} prefers to coordinate with DMSO, thus the complex structure changes. In addition, DMSO has strong interaction with water, which deactivate water molecules and suppress the water splitting. The battery cycling life is much longer with the help of DMSO, however, the overpotential goes up at the same time. Although Zn^{2+} prefers to coordinate with DMSO and replaces water out of the complex structure, the desolvation step should turn even more difficult and may consume more energy due to the stronger interaction coming with preference. While Qiao et al. introduces methanol (MeOH) as additive inside electrolyte[35], as it is shown in Figure 3. Since MeOH has a similar Gutmann doner number (19) with water[36], Zn^{2+} has no preferential coordination with MeOH nor water. In other words, the complex structure is defined by the dominate solvent, thus the coordinated water in $[Zn(H_2O)_6]^{2+}$ is replaced by coordinated MeOH if 50% MeOH is added inside the electrolyte. However, MeOH is toxic and highly volatile, which is also an inevitable disadvantage.

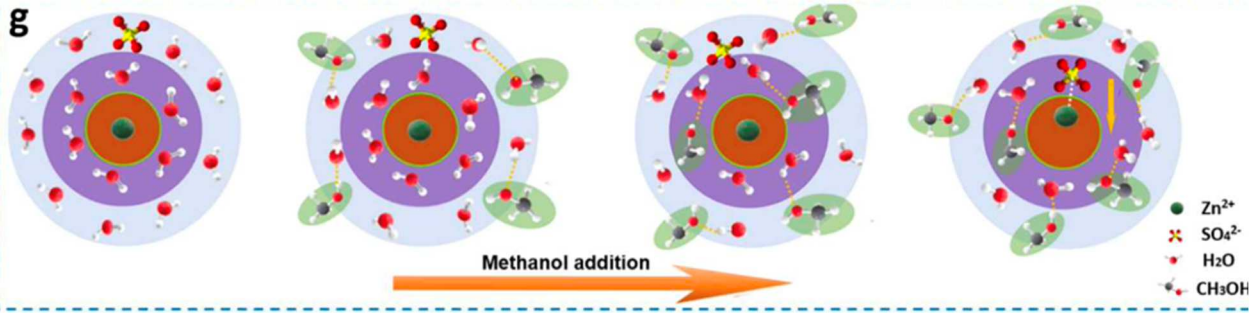

Figure 3. The effect of methanol additive into electrolyte from Ref.35

Researchers are also working on interfacial engineering, which modifies the property of interface by creating another interface in order to accelerate the desolvation process. Wang et al. also tried to create a hydrophobic interface on the electrode[37]. As it is shown in Figure 4, the bulk electrolyte is aqueous $Zn(TFSI)_2$, while the hydrophobic interface is made of $Zn(TFSI)_2$ dissolved in tris(2,2,2□trifluoroethyl)phosphate (TFEP), immobilized on a metal-organic frameworks (MOFs) material HKUST-1. Though the cycling life is improved, using expensive salt and toxic organic solvent is not applicable. What's worse, creating a heterogenous interface increases the resistance for Zn^{2+} diffusion.

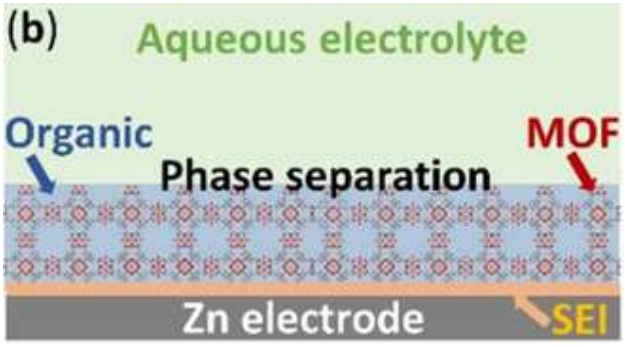

Figure 4. The effect of methanol additive into electrolyte from Ref.37

Zhou et al., on the other hand, uses another Zn-based MOFs material (ZIF-7) directly coated on the electrode surface[32], as it is showed in Figure 5. It is very surprising that ZIF-7 channel creates super-saturated electrolyte proved by Raman spectrum. This MOFs coating prolongs the cycling life of Zn vs Zn symmetric battery and Zn vs MnO_2 battery, however, it is not clearly revealed that how ZIF-7 helps to desolvate the $[Zn(H_2O)_6]^{2+}$ rapidly. Additionally, the coating process is not convenient process. Hydrophobic poly vinylidene fluoride (PVDF) is used as binder, firstly dissolved in Dimethylformamide (DMF) and then mixed with ZIF-7 powders based on the 1:3 mass ratio. Finally, DMF needs drying after the coating process. This process is complex and it introduces hydrophobic binder into the aqueous system, which results in an increasing overpotential when compared with a bare Zn vs Zn symmetric battery.

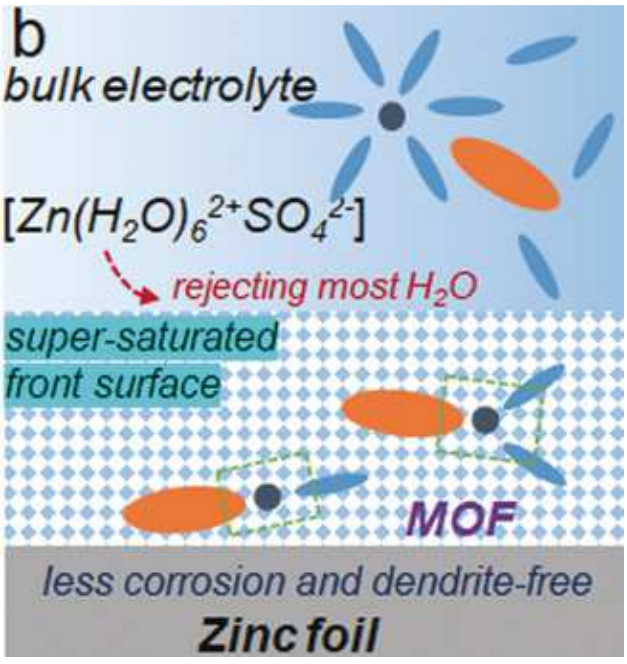

Figure 5. The effect of MOF coating on the electrode from Ref.32

MOFs is a new class of material composed of modular structures (i.e., ions and organic linkers) which offer great diversity in tunnel structures and tailored properties[38]. As the pioneer in MOFs material in the world, Yaghi et al. introduced a new group of MOFs materials which is Zr-based ones[39], and they have huge potential to be used in water capture and release under desert environment due to three important standards: (1) water condensation at a relatively low pressure; (2) high stability in water; (3) high reversibility (i.e., easy adsorption and desorption of water). Compared with Zr-based MOFs materials, zeolitic imidazolate framework (ZIF) including the aforementioned ZIF-7 has strong interaction with water and might create hard barrier of desorption of water. MOFs additive or coating should improve the desolvation process by absorption of water during the charging process, however, it should also have reversibility of releasing water to prevent deterioration of the solvation process during the discharge since ZIB battery is targeted reversible.

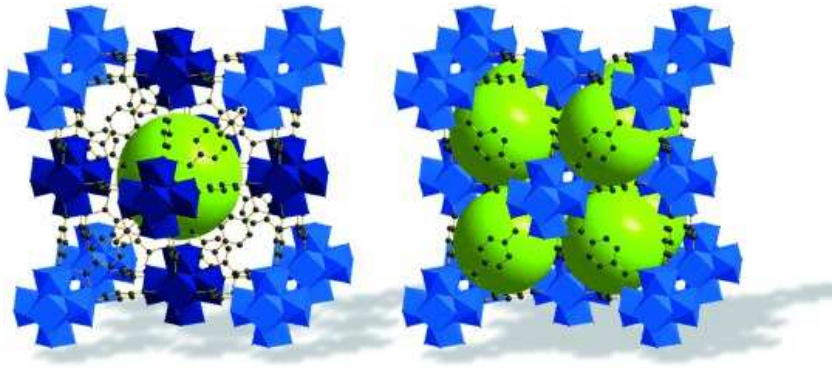

Figure 6. The structure of UIO-66 from Ref.41, where blue represents the Zr clusters, and green ball represents the space in the frameworks.

Among all the Zr-based MOFs materials, UIO-66 and MOF-808 are the combination of Zr secondary building units (SBUs) and the two easiest, cheapest organic linker 1,4-

Benzenedicarboxylic acid (H_2BDC) and Benzene-1,3,5-tricarboxylic acid (H_3BTC) respectively, originating from a mild synthesis condition[39,40]. As it is showed in Figure 6, UIO-66 is the combination of $[Zr_6O_4(OH)_4(CO_2)_{12}]$ SBUs clusters and H_2BDC acid. The $[Zr_6O_4(OH)_4(CO_2)_{12}]$ SBUs clusters occupy the sites of a facial center cubic lattice, and H_2BDC acid works as the bridge connecting the clusters [41]. UIO-66 has showed great properties in a variety of applications such as gas captures[41] and photocatalysis[42].

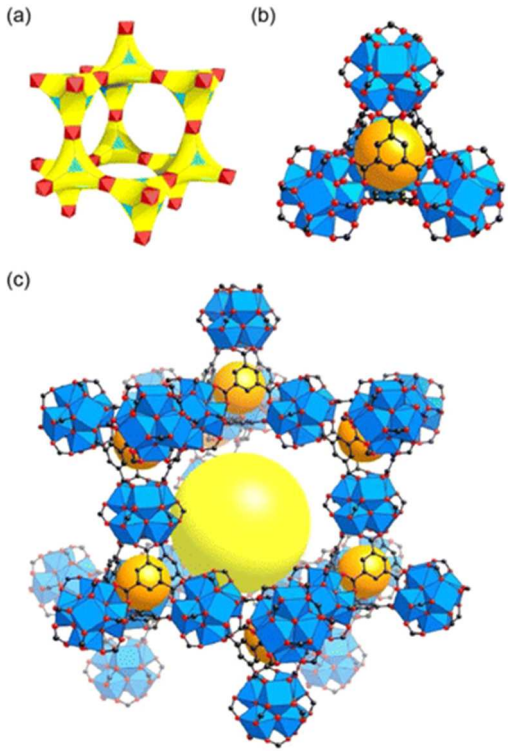

Figure 7. The structure of MOF-808 from Ref.40, Atom color scheme: Zr, blue polyhedral; C, black; O, red; and orange ball represents the space in the frameworks.

MOF-808 is the combination of $[Zr_6O_4(OH)_4(CO_2)_6]$ SBUs clusters and H_3BTC acid. As it is showed in Figure 7, The $[Zr_6O_4(OH)_4(CO_2)_6]$ SBUs clusters occupy the 4 sites of a tetrahedral

unit, and H_3BTC acid works as the bridge connecting the clusters[40]. MOF-808 has also showed great properties in a variety of applications such as proton conducting[43] and heavy metal ion removal[44].

MOF is not only famous for their customizable SBUs, organic linkers and channel topography, but also famous for their open metal sites (OMSs). Generally, these OMSs are occupied by solvent molecules, which yet can be removed by vacuum heating (activation). The unoccupied OMSs are very active, and can capture other solvents or anions, thus the target material is likely to be immobilized on MOFs. Luo et al. used MOFs to capture task specific ionic liquid (TSIL) for catalysis[45,46]. The MOFs cage serves as the house for ionic liquid catalyst, and OMSs serve as the "anchor" point for the anion of ionic liquid. This immobilizes the ionic liquid catalyst and avoids its outflow to the organic solvent, which is beneficial for the catalyst recycle. Lu et al. has tried to immobilize the $LiPF_6$, $LiClO_4$ or Lithium bis(trifluoromethanesulfonyl)imide (LiTFSI) on UIO-66 or HKUST-1 MOFs material[47-49]. Compared with the neutral solvents, the negatively charged anions has larger potential to be absorbed to the OMSs. The immobilization of anion is beneficial to accelerate the single Li^+ conductivity, whose influence is the enhancement of Li^+ transference number, rate capability and cycling life. Those applications of OMSs of MOFs are promising.

Instead of making a film coating, consuming a large amount of ZIF-7 additive and introducing the hydrophobic binder PVDF[32], herein, a small amount of Zr-based MOFs powder, including UIO-66 and MOF-808, will be dropped and spread evenly into the bulk aqueous $ZnSO_4$ solution, which generates an easier manufacture procedure and a possibly reversible desolvation and solvation process. The development of Zn vs Zn symmetric battery testing platform will be discussed to clarify all the details which might have huge influence on the battery performance.

Additionally, the effect of MOFs additive concentration, the effect of MOFs species and the effect of activation temperatures (the effect of MOFs open metal sites) will be discussed with the help of Zn vs Zn symmetric battery testing result (overpotential) and electrochemical impedance spectroscopy (EIS). A result can be regarded better when overpotential is smaller, cycling life is longer and charge transfer impedance is smaller on EIS Nyquist plot.

2 Method

2.1 Synthesis

2.1.1. UIO-66

UIO-66 is solvothermally synthesized in accordance with the Farha's paper[40]. 375 mg $ZrCl_4$, 369mg 1,4-Benzenedicarboxylic acid (H_2BDC), 3 ml HCl and 45 ml DMF are sonicated in a 60 ml Teflon lined vessel, which is later transferred to an autoclave and crystallized at 80 °C for 24 hours. The resulting solid is exchanged with 3 times DMF and 3 times methanol afterwards, with an 8-hour gap. Finally, the solid is dried in 60 °C oven for 2 hours and named after UIO-66 (room).

In order to generate open metal sites, UIO-66 is activated in vacuum environment for 24 hours under 300 °C or 120 °C. And the solids are named after UIO-66 (300C) and UIO-66 (120C), respectively.

2.1.2. MOF-808

MOF-808 is solvothermally synthesized in accordance with Yaghi's paper[39]. 800 mg $ZrOCl_2 \cdot H_2O$, 550 mg Benzene-1,3,5-tricarboxylic acid (H_3BTC), 100 ml HCOOH and 100 ml DMF are sonicated 30 minutes in a 300 ml screw-capped glass jar, which is later transferred to an oven and crystallized at 120 °C for 48 hours. The resulting solid is exchanged with 9 times DMF and 9 times acetone with an 8-hour gap. Finally, the solid is dried in 60 °C oven for 2 hours and named after MOF-808 (room).

In order to generate open metal sites, MOF-808 is activated in vacuum environment for 24 hours under 300 °C or 120 °C. And the solids are named after MOF-808 (300C) and MOF-808 (120C), respectively.

2.1.3. Electrolyte

2M $ZnSO_4$ is used as standard electrolyte for Zn vs Zn symmetric battery.

MOFs is added inside the electrolyte based on weight percentage 1wt%, 2wt% and 5wt%, and then the mixture is stirred for 15 minutes at room temperature before making the battery. The electrolyte is kept in a glass vial which should be screwed tightly to prevent evaporation after used.

2.2 Characterization

2.2.1. X-ray diffraction (XRD)

The X-ray diffraction (XRD) measurements were taken by a Rigaku X-ray powder diffractometer with copper Kα radiation (λ = 1.54 Å). During the analysis, the sample was scanned from 3 to 80 ° at a speed of 5 degree per minute.

2.2.2. N_2 sorption/desorption measurements

N_2 sorption/desorption measurements were conducted by Micromeritics ASAP 2020 system at 77 K. All samples were degassed at 120 °C vacuum oven overnight before tested.

2.2.3. Thermogravimetric analysis (TGA)

Thermogravimetric analysis (TGA) curves were obtained from a TA Q50 thermogravimetric analyzer. The samples were heated in air atmosphere with a heating rate of 10 °C per minute until 600 °C.

2.2.4. Electrochemical Impedance Spectroscopy (EIS)

Electrochemical Impedance Spectroscopy (EIS) is used for testing the charge transfer impedance of Zn^{2+}. Glass fiber separator was cut into 18.5-millimeter-diameter disk, and Zn disk electrode was cut into 16-millimeter-diameter disk. Then Zn disk electrode, 50 μl electrolyte, separator, 50 μl electrolyte and Zn disk electrode are sandwiched in order into a symmetric Zn vs Zn coin cell battery. The testing program is set with an alternating current (AC) amplitude of 15 mV and a frequency from 10^6 to 1 Hz. The test should be repeated until two recent curves relatively overlap.

EIS curves under different temperatures are also collected. During the test, the Zn vs Zn coin cell battery is placed inside the oven with the temperature of 40 °C, 45 °C, 50 °C and 55 °C. The test should not be started until 5 minutes later after the oven reaches the setting temperature.

2.3 Battery testing program

The LAND battery testing system is used for measuring the performance of battery. Constant areal current densities on the effective area of Zn electrode 0.25 mA/cm^2, 0.50 mA/cm^2 and 1.00 mA/cm^2 were added. Each cycle in the battery test starts with one-hour discharge and ends with one-hour charge. By changing the cycles for different current densities in the testing

program, the stability of Zn vs Zn symmetric battery under low, middle, and high current densities will be obtained.

3 Foundation of the Zn-ion battery testing platform

3.1 Importance

Since this is the first time that Prof. Yunfeng Lu's lab has made research on zinc-ion coin cell battery, all the details of making a successful zinc-ion coin cell battery should be discussed. A testing result is influenced by scientific factors (the chemical properties) and non-scientific factors (the details of making the coin cell battery), thus it is extremely vital to find out these factors, their influences and make non-scientific factors and certain irrelevant scientific factors most optimized. This is the only way in which a persuasive conclusion can be made when certain comparison experiments showed difference in performance. This thesis mainly focuses on the Zn vs Zn symmetric battery, whose performance shows the overpotential during charging and discharging.

3.2 Zn vs Zn symmetric battery in a beaker cell testing platform

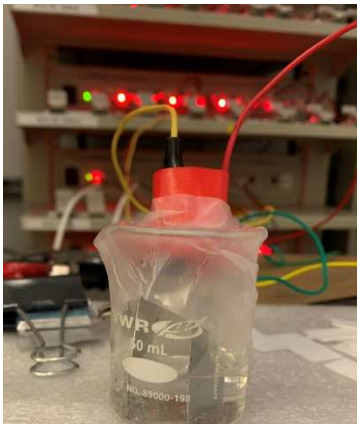

Figure 8. The beaker cell testing platform

Beaker cell is the most primitive testing platform, as it is shown in Figure 8, thus the reversibility of the Zn vs Zn symmetric battery showed on beaker cell testing platform is only

influenced by the reversibility of chemical reaction. In addition, the overpotential of Zn vs Zn symmetric battery showed on beaker cell testing platform is only influenced by the reaction as well.

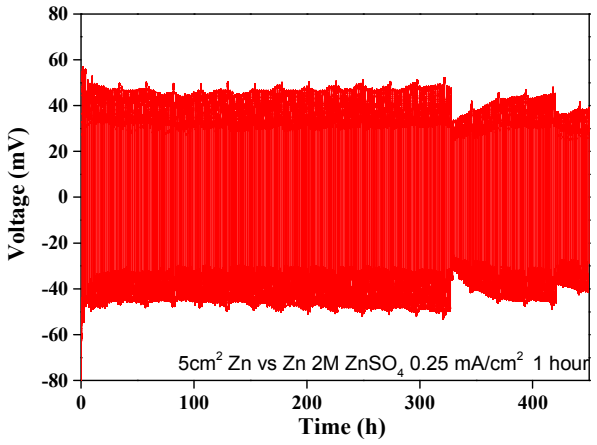

Figure 9. The result of beaker cell testing platform

The testing result in Figure 9 shows that the Zn vs Zn symmetric battery is reversible and the overpotential should be around 60 mV. The results coming from the other testing platforms afterwards should be compared with that in beaker cell testing platform.

3.3 Zn vs Zn symmetric battery in a pouch cell testing platform

Pouch cell is a semi-modern testing platform. Compared with beaker cell, pouch cell has the separator, which significantly decreases the distance between two electrodes and the amount of electrolyte. Two Zn electrodes were both firstly cut into 2.5 cm*4 cm rectangle shape and then a 2 cm*2 cm square is cut out of the rectangle, leaving an effective area of 2.5 cm*2 cm and a connecting area (to testing system) of 0.5 cm*2 cm.

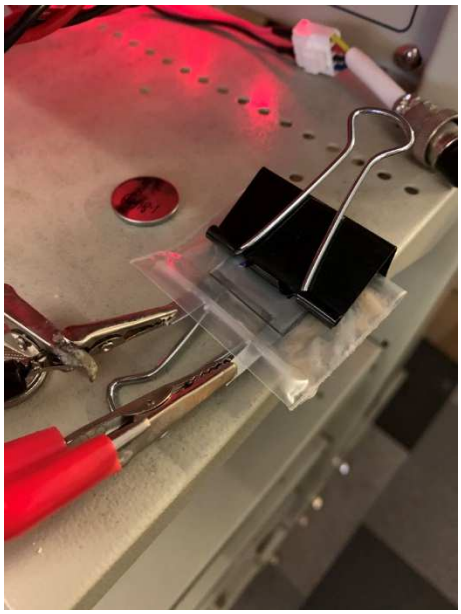

Figure 10. The pouch cell testing platform

Polypropylene (PP) and glass fiber (GF) are currently the two common separators in the lab, and they are both cut into 3 cm*2.5 cm rectangle shape, which is large enough to separate two electrodes. Then Zn electrode, 250 µl electrolyte, separator, 250 µl electrolyte and Zn electrode are sandwiched in order in a plastic zip reclosable bags, and two 2.5 cm*2 cm effective areas should overlap. Finally, as it is shown in Figure 10, two pieces of glass and a clip are added on the effective area, which generates a facial pressure to stabilize the electrodes and maintain the effective area.

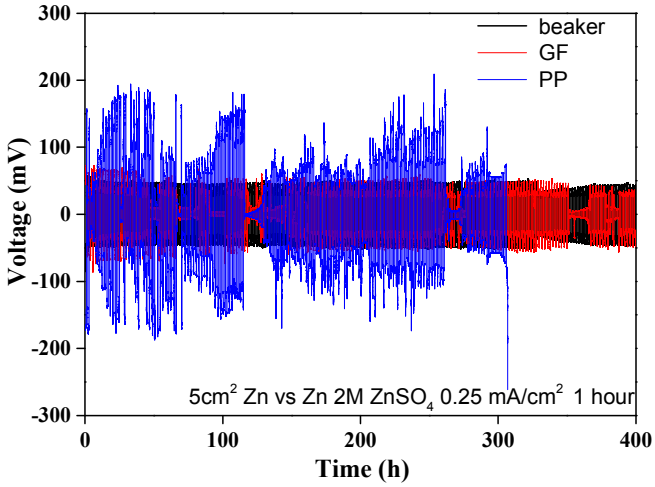

Figure 11. The effects of different separators in pouch cell testing platform

Figure 11 shows the results of two different separators, and it is clearly seen that glass fiber (GF) should be the suitable separator because the overpotential is almost the same with that in beaker cell and the longevity can be guaranteed. Polypropylene (PP), however, increases the overpotential and decreases the cycling life.

It is also unexpectedly found that pressure has a great influence on cycling life as well. As it is shown in Figure 12, Zn vs Zn pouch cell with glass fiber can have short circuit during the cycling process, forming a constant voltage during both discharge and charge steps. However, the Zn vs Zn symmetric battery returns normal when the pressure of clip is removed, forming a normal peak again.

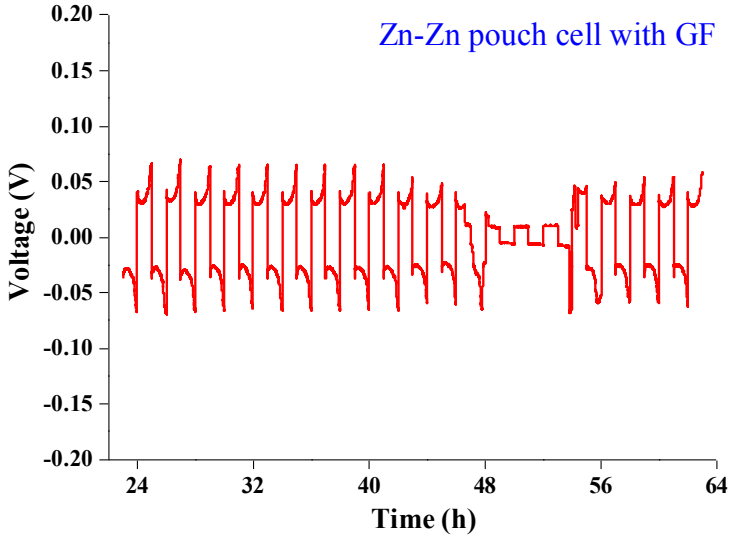

Figure 12. The effect of pressure in pouch cell testing platform

Figure 13 shows that when pouch cell battery is dissembled, the center area of glass fiber separator (facing the Zn electrode effective area) is almost dry, whereas the edge of glass fiber separator is saturated with electrolyte. The reason is that glass fiber is extremely hydrophilic like a cloth, and pressure can squeeze the electrolyte out of the glass fiber. This gives an extremely important lesson for assembling the coin cell battery that a suitable pressure is highly crucial for the longevity of Zn vs Zn symmetric battery with glass fiber.

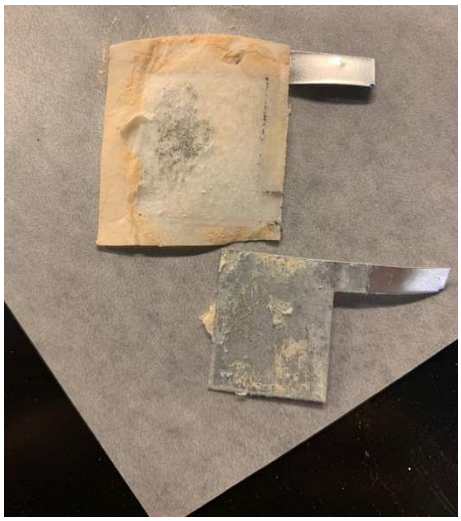

Figure 13. The effect of pressure in pouch cell testing platform

All in all, with pouch cell testing platform, it is found that glass fiber is the suitable separator of Zn vs Zn symmetric battery and pressure on the battery has a huge impact on the cycling life. However, the pouch cell testing platform has the following unacceptable disadvantages.

First, this testing platform consumes much zinc resources. In a coin cell system, 16-millimeter-diameter disk electrode is often used, which is only 2.01 cm^2, while 2.5 cm*4 cm rectangle Zn electrode is used in pouch cell testing platform and that is 4 times more consumption than a disk electrode.

Second, this pouch cell platform is not fully closed due to the Zn connecting area, whose result is that the electrolyte can evaporate very slowly and then changes the electrolyte concentration and MOFs additive concentration.

Third, though removal of the pressure of the clip guarantees the cycling life, the electrode cannot be stabilized, which means it might have rotation or translation and then changes the effective area.

Updating the pouch cell testing platform into coin cell testing platform is crucial.

3.4 Zn vs Zn symmetric battery in a coin cell testing platform

Coin cell battery is a modern testing platform. Compared with pouch cell testing platform, coin cell is a mini testing platform using components such as anode cap and cathode cap, which fully encloses the electrolyte in a much smaller space, thus consumes less electrolyte as well. Given that Zn vs Zn symmetric battery is absolutely non-sensitive to oxygen and moisture, assembly of the coin cell battery can be processed under a normal room environment. For most convenience, 16-millimeter-diameter zinc electrode, which is the biggest disk electrode allowed in a coin cell, is used in the following experiments. When this big disk electrode is placed inside, it can be exactly in the middle of the center without much careful adjustment. Big disk electrode also reduces the risk of electrode translation during the assembly and the risk of short circuit afterwards

Glass fiber separator is cut into 18.5-millimeter-diameter disk, and Zn disk electrode is cut into 16-millimeter-diameter disk. Then Zn disk electrode, 50 μl electrolyte, separator, 50 μl electrolyte and Zn disk electrode are sandwiched in order in a coin cell. It has been discussed that a big pressure can deteriorate the cycling life of the Zn vs Zn symmetric battery by squeezing out the electrolyte in glass fiber. However, a small pressure might result in a poor contact among electrodes, glass fiber separator and coin cell components, which increases the impedance. In addition, a small pressure is not enough to eliminate leakage of coin cell and the electrolyte can evaporate like the aforementioned condition. A pressure of 700 psi is the most optimized one when assembling coin cell for Zn vs Zn symmetric battery. What is more, coin cell space control and adjustment by adding different coin cell plate is very important as well in order to give a close contact among electrodes, glass fiber separator and coin cell components.

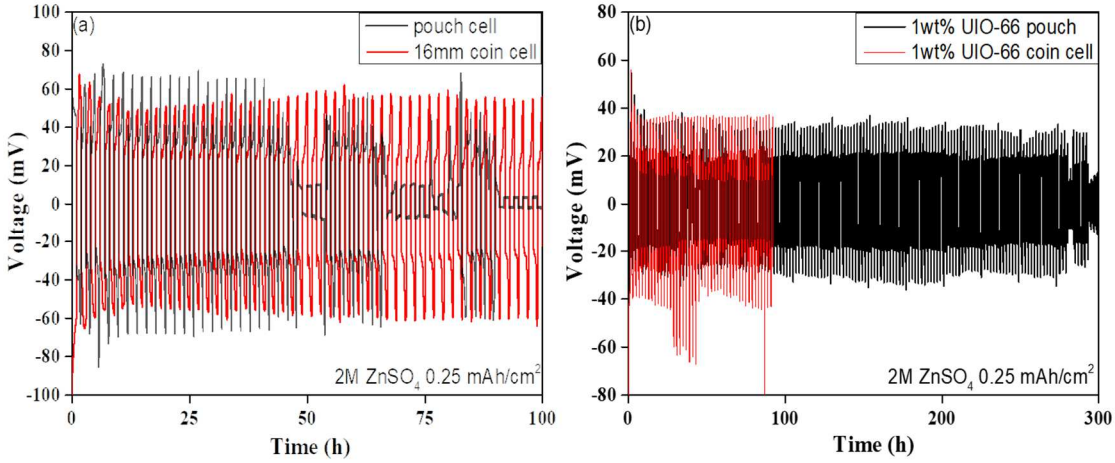

Figure 14. The comparison between pouch cell testing platform and beaker cell testing platform of Zn vs Zn symmetric battery with electrolyte made by (a) 2M $ZnSO_4$ and (b) 2M $ZnSO_4$ plus 1wt% UIO-66 additive

From Figure 14, it is clearly seen that Zn vs Zn symmetric battery with standard 2M $ZnSO_4$ electrolyte in the coin cell platform has the similar performance with that in the pouch cell platform. When UIO-66 MOFs additive is added inside, the performance of two battery systems is similar as well. In conclusion, the coin cell battery platform is successfully set up.

4 Results and Discussion

4.1 MOF material characterization

4.1.1. X-ray diffraction (XRD)

The XRD patterns for UIO-66 and MOF-808 are showed in Figure 15. UIO-66 shows intense peaks around 7.3°, 8.5° and 25.6°, which confirms its existence. While MOF-808 shows intense peaks around 4.3°, 8.3°, 8.7° and 10.0°, which has accordance with the paper.

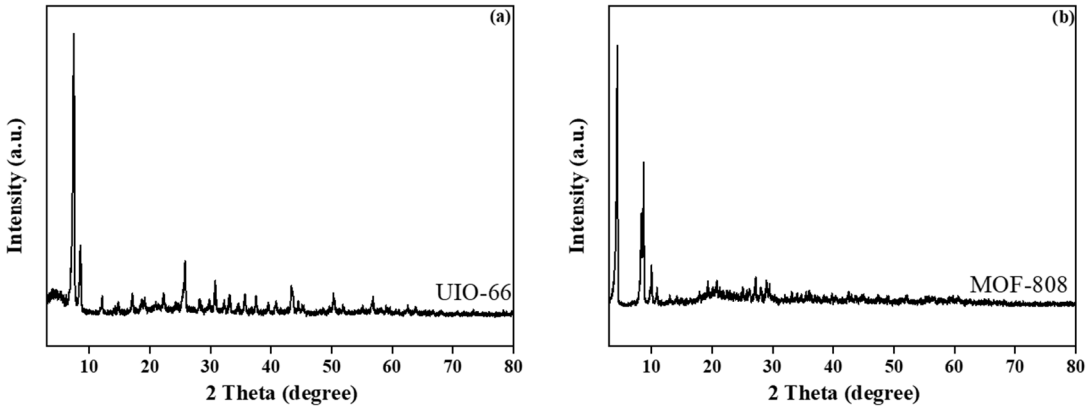

Figure 15. The XRD result of (a)UIO-66 and (b)MOF-808

4.1.2. N_2 sorption/desorption measurements

N_2 sorption/desorption measurements were conducted to see the surface area and pore distribution of UIO-66 and MOF-808. By choosing the Brunauer-Emmett-Teller (BET) model, the isothermal adsorption result of UIO-66 and MOF-808 is showed in Figure 16. UIO-66 exhibits a

surface area of 1027 m^2/g and 0.54 cm^3/g (1390 m^2/g and 0.70 cm^3/g reported[50]), while MOF-808 exhibits a surface area of 1470 m^2/g and 0.71 cm^3/g (2060 m^2/g and 0.84 cm^3/g reported[39]).

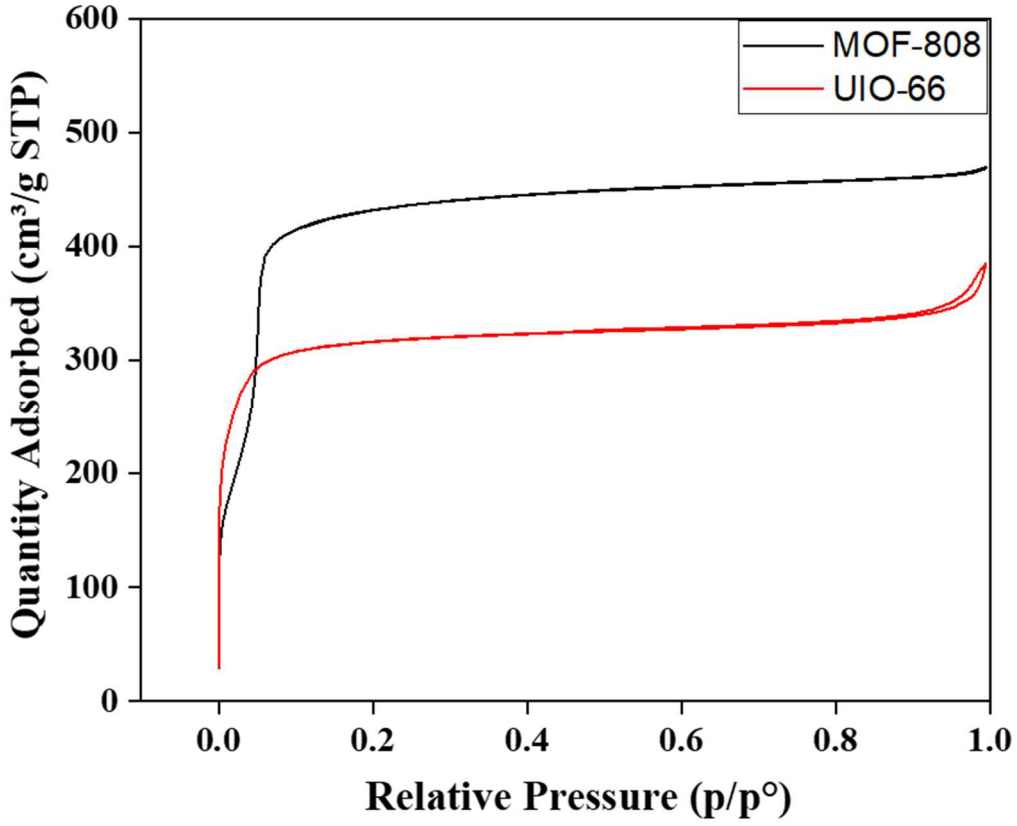

Figure 16. The BET isotherm adsorption result of UIO-66 and MOF-808

4.1.3. Thermogravimetric analysis (TGA)

Figure 17 shows the TGA graph of UIO-66 and MOF-808, indicating their thermostabilities. It can be seen that UIO-66 and MOF-808 can still maintain 90% of their own original weights respectively when the temperature is below 300 °C, where most weight loss is attributed to solvent loss. When the temperature is over 300 °C, MOF-808 loses weight rapidly at once, indicating its decomposition. Thus, 300 °C is the highest temperature limit for MOF-808

when it is vacuum-dried (activated). In order to make comparison, 300 °C is the highest temperature limit for UIO-66 when it is vacuum-dried (activated) as well.

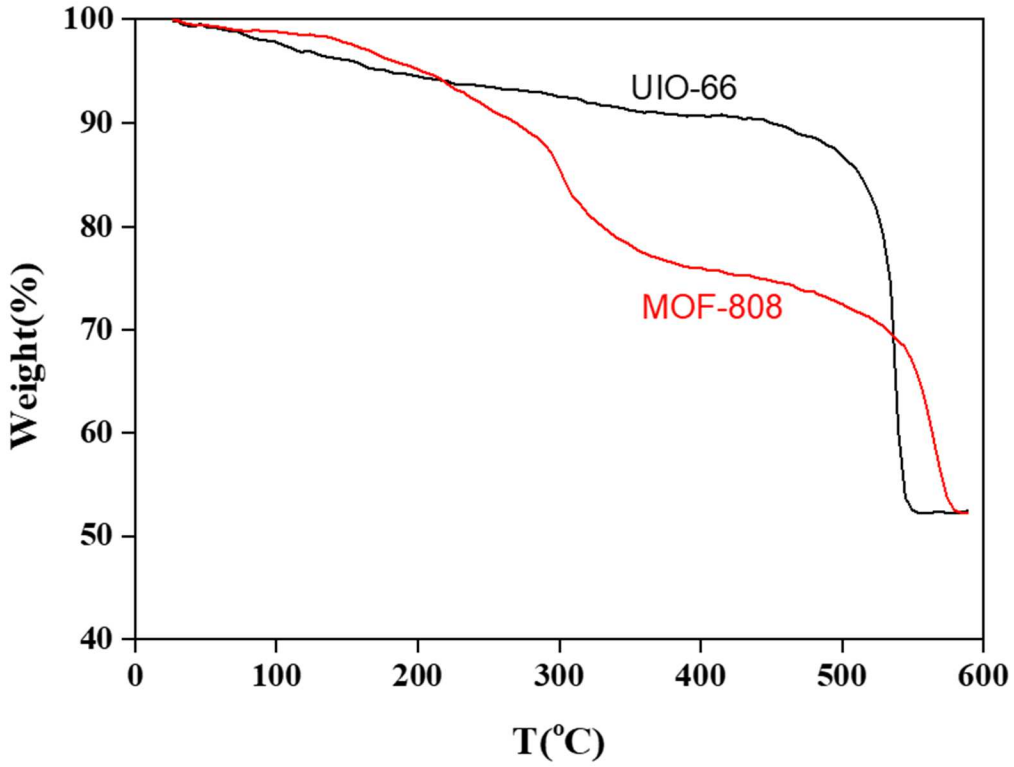

Figure 17. The TGA result of (a)UIO-66 and (b)MOF-808

4.2 Battery Performance

4.2.1. The effect of MOF additive concentration

The effect of different concentrations of MOF additive was investigated. As Figure 18 shows, though the UIO-66 additive in the Zn vs Zn symmetric battery in a coin cell testing system helps decrease the overpotential, different concentrations of UIO-66 additive show little difference on performance. There is also a critical additive concentration 10wt%, above which the coin cell

will not be assembled successfully. In the following experiment, the concentration of MOFs additive was maintained at 2wt%.

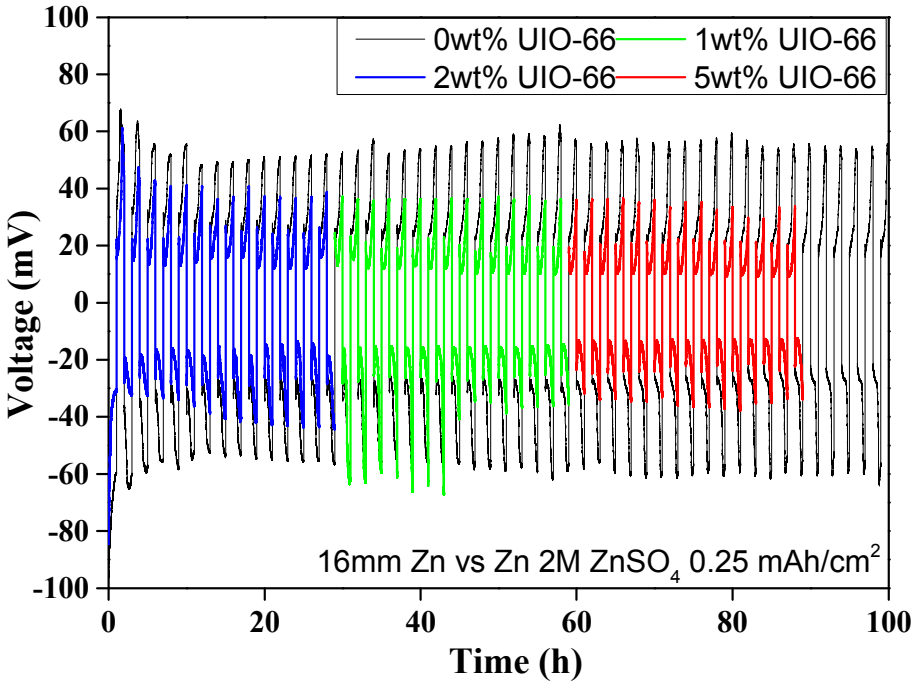

Figure 18. The comparison results of Zn vs Zn symmetric battery cycling performance with different concentrations of UIO-66 additive

4.2.2. The effect of UIO-66 additive activation temperature

The effect of different activation temperatures of UIO-66 additive was investigated. Constant areal current densities were added on the effective area of Zn electrode: 0.25 mA/cm^2 for 50 cycles, 0.50 mA/cm^2 for another 50 cycles and 1.00 mA/cm^2 for later continuous test. Each cycle in the battery test starts with one-hour discharge and ends with one-hour charge.

Figure 19 shows how activation temperature of UIO-66 additive influences the performance of Zn vs Zn symmetric battery. In Figure 19(a), the Zn vs Zn symmetric coin cell

battery made with standard 2M $ZnSO_4$ electrolyte exhibits an unstable overpotential which is over 150 mV, and its cycling life is only 150 hours.

Compared with Figure 19(a) made by standard 2M $ZnSO_4$ electrolyte, with the help of 2wt% UIO-66(300C) additive, the overpotential under the current density of 0.25 mA/cm^2 showed in Figure 19(b) is decreased hugely from over 150 mV to 50 mV, which is 67% smaller. UIO-66 is surely helpful to regulate and stabilize the overpotential, thus it is surely beneficial to regulate and stabilize the interface. However, its longevity unexpectedly cannot be maintained before the current density increases from 0.25 mA/cm^2 to 0.50 mA/cm^2.

Compared with Figure 19(b) made by standard 2M $ZnSO_4$ electrolyte plus 2wt% UIO-66(300C), standard 2M $ZnSO_4$ electrolyte plus 2wt% UIO-66(120C) gives better battery performance, as it is showed in Figure 19(c). The overpotential under the current density of 0.25 mA/cm^2 is slightly bigger than 50 mV but can be maintained. As the current density goes up to 0.50 mA/cm^2, the overpotential roughly increases to 75 mV and is stable for another 100 hours. Finally, as the current density goes up to 1.00 mA/cm^2, the overpotential roughly increases to 100 mV and is stable for another 180 hours. The overpotential drops down later and shows extremely flat on the top, representing the battery ends up with short circuit.

It is normal that the overpotential increases with the increasing current density because the electronic conductivity inside the electrode metal side is faster than the ionic conductivity which includes bulk ionic conductivity and interfacial ionic conductivity. The interfacial ionic conductivity is likely influenced by ionic diffusion through the interface and the desolvation of $[Zn(H_2O)_6]^{2+}$, both of whose sluggish rate can decrease the interfacial ionic conductivity. Thus, the electron or “positive charge” shall accumulate on the electrode as the current density increases,

which causes overpotential bigger. Overall, 2wt% UIO-66(120C) gives a rather good reversibility for Zn vs Zn symmetric battery.

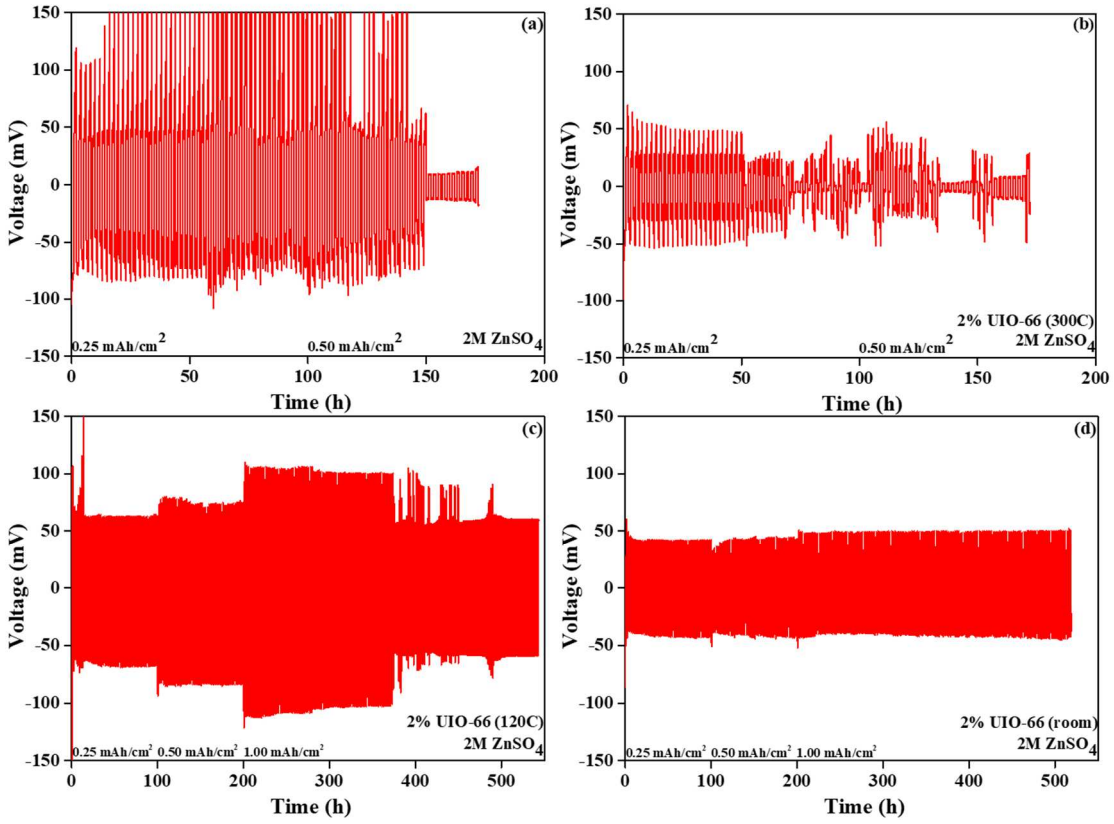

Figure 19. The comparison result of Zn vs Zn symmetric battery cycling performance with UIO-66 additive under different activation temperatures (a) 2M $ZnSO_4$ without UIO-66 (b) 2M $ZnSO_4$ plus 2wt% UIO-66 (300C) additive (c) 2M $ZnSO_4$ plus 2wt% UIO-66 (120C) additive (d) 2M $ZnSO_4$ plus 2wt% UIO-66 (room) additive

However, compared with Figure 19(c) made by standard 2M $ZnSO_4$ electrolyte plus 2wt% UIO-66(120C), standard 2M $ZnSO_4$ electrolyte plus 2wt% UIO-66(room) gives amazingly better battery performance, as it is showed in Figure 19(d). The overpotentials under the current density

of 0.25 mA/cm^2, 0.50 mA/cm^2 and 1.00 mA/cm^2 are all around 50 mV roughly, and the battery life can last over 250 hours. The possible reason is that 2wt% UIO-66(room) accelerates the desolvation step, thus the overpotential will not increase with the increasing current density when the desolvation step is probably not the rate-determining step any more.

In summary, standard 2M $ZnSO_4$ electrolyte plus 2wt% UIO-66 additive activated in different temperatures are tested in Zn vs Zn symmetric battery. The higher activation temperature the UIO-66 is applied with, the worse battery reversibility exhibits. 2wt% UIO-66(room) shows the best performance with an almost constant overpotential under the current density of 0.25 mA/cm^2, 0.50 mA/cm^2 and 1.00 mA/cm^2.

4.2.3. The effect of MOF-808 additive activation temperature

The effect of different activation temperatures of MOF-808 additive was investigated. Similarly, constant areal current densities were added on the effective area of Zn electrode: 0.25mA/cm^2 for 50 cycles, 0.50 mA/cm^2 for another 50 cycles and 1.00 mA/cm^2 for later continuous test. Each cycle in the battery test starts with one-hour discharge and ends with one-hour charge.

Figure 20 shows how activation temperature of MOF-808 additive influences the performance of Zn vs Zn symmetric battery. Figure 20(a) is the same with Figure 19(a), where the Zn vs Zn symmetric coin cell battery made with standard 2M $ZnSO_4$ electrolyte exhibits an unstable overpotential which is over 150 mV, and its cycling life is only 150 hours.

Compared with Figure 20(a) made by standard 2M $ZnSO_4$ electrolyte, with the help of 2wt% MOF-808(300C) additive, the overpotential under the current density of 0.25 mA/cm^2 showed in Figure 20(b) is decreased hugely from over 150 mV to 75 mV, which is 50% smaller.

MOF-808 is also surely helpful to regulate and stabilize the overpotential, thus it is surely beneficial to regulate and stabilize the interface. However, its longevity unexpectedly cannot be maintained before the current density increases from 0.25 mA/cm^2 to 0.50 mA/cm^2, and only lasts for 100 hours.

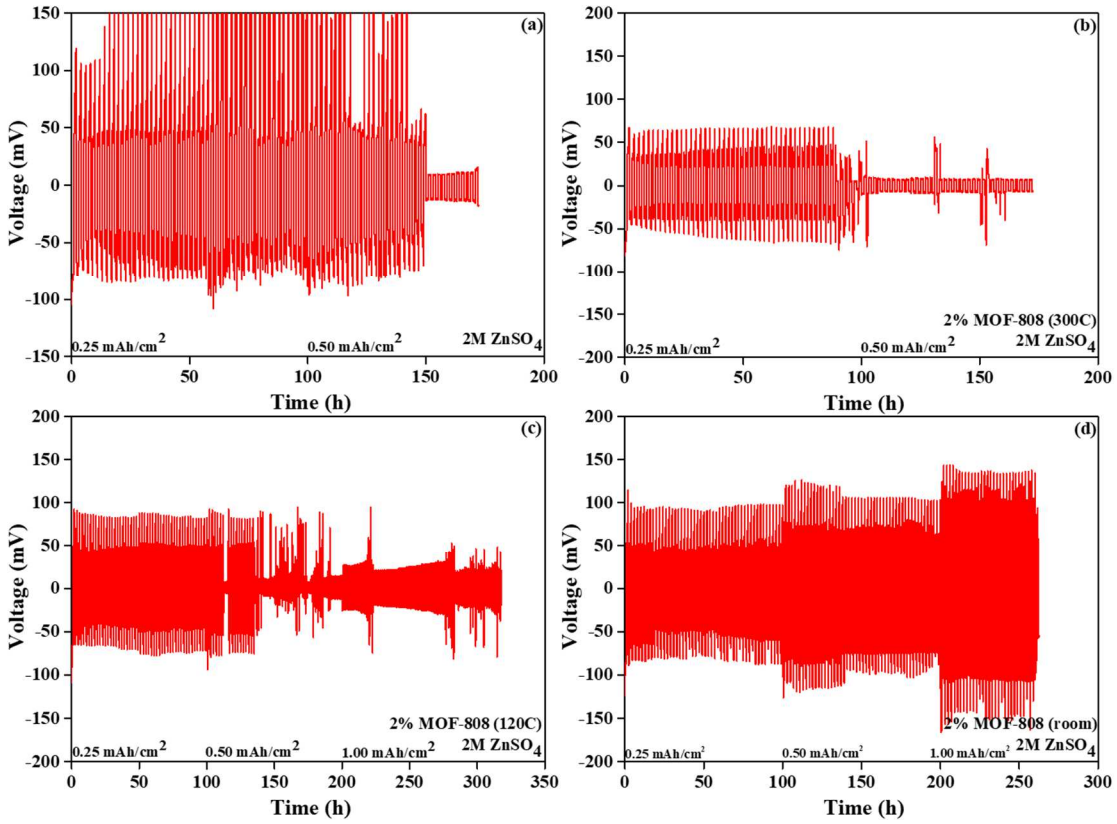

Figure 20. The comparison result of Zn vs Zn symmetric battery cycling performance with MOF-808 additive under different activation temperatures (a) 2M $ZnSO_4$ without MOF-808 (b) 2M $ZnSO_4$ plus 2wt% MOF-808(300C) additive (c) 2M $ZnSO_4$ plus 2wt% MOF-808(120C) additive (d) 2M $ZnSO_4$ plus 2wt% MOF-808(room) additive

Compared with Figure 20(b) made by standard 2M $ZnSO_4$ electrolyte plus 2wt% MOF-808(300C), standard 2M $ZnSO_4$ electrolyte plus 2wt% MOF-808(120C) does not give better battery performance, as it is showed in Figure 20(c). This result is not consistent with UIO-66(120C) over UIO-66(300C). Under the same initial current density 0.25 mA/cm^2, 2wt% MOF-808(120C) makes the overpotential reach 100 mV, which is higher (worse) than that of 2wt% MOF-808(300C). Even though the overpotential does not increase much after the current density increases to 0.50 mA/cm^2, the cycling life only extends for another 30 hours.

Compared with Figure 20(c) made by standard 2M $ZnSO_4$ electrolyte plus 2wt% MOF-808(120C), standard 2M $ZnSO_4$ electrolyte plus 2wt% MOF-808(room) gives better battery performance, as it is showed in Figure 20(d). The overpotential increases with the increasing current density, however, the cycling life is good. This result is not the same with the result of UIO-66(room), but it is similar to the result of UIO-66(120C).

In summary, standard 2M $ZnSO_4$ electrolyte plus 2wt% MOF-808 additive activated in different temperatures are tested in Zn vs Zn symmetric battery, and the higher activation temperature the MOF-808 is applied with, the worse battery reversibility exhibits. The 2wt% MOF-808(120C) should have been better, but it does not reach the expectation for some unknown reason. 2wt% MOF-808(room) shows the best performance in cycling life, and its overpotential increases with the increasing current density.

Up to now, the effect of activation temperature of UIO-66 and MOF-808 have both been discussed. It is noticed that there is the same conclusion that the higher MOFs activation temperature deteriorates the battery performance and longevity. According to the aforementioned introduction part, high temperature can help MOFs generate open-metal sites (OMSs), which are exposed with the removal of solvent in MOFs pores. This is beneficial for Li-ion battery for

immobilizing the anions, but it seems not good for aqueous Zn^{2+} battery because its mechanism is more closely related to desolvation during charge and solvation during the discharge. In order to make the Zr-MOFs additive as a reversible layer for solvent-exchange process, non-activated MOFs should likely be the best.

4.2.4. The effect of MOF species

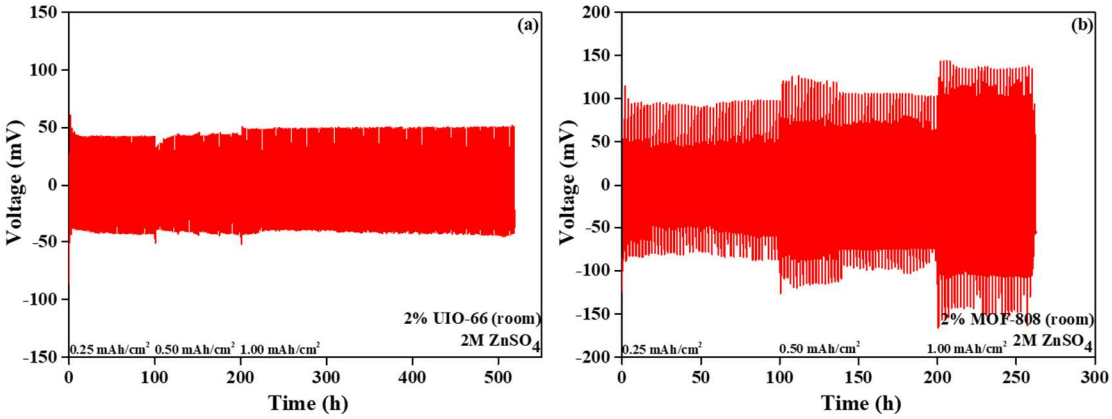

Figure 21. The comparison result of Zn vs Zn symmetric battery cycling performance (a) 2M $ZnSO_4$ plus 2wt% UIO-66 (room) additive (b) 2M $ZnSO_4$ plus 2wt% MOF-808 (room) additive

The above part has just discussed that MOFs additive without activation, including UIO-66(room) and MOF-808(room), have the best results in their own groups. However, if they are compared with each other, according to Figure 21, the overpotential of electrolyte with UIO-66(room) is 50% smaller than that with MOF-808(room). What is more, the overpotential of electrolyte with UIO-66(room) does not obviously increase with the increasing current density. According to the analysis in part 4.3.2, the possible reason is that the UIO-66 (room) makes the desolvation resistance small enough to not be the rate-determining step, and then makes the

overpotential irrelevant with current density. However, the overpotential of electrolyte with MOF-808(room) still increases with the increasing current density, indicating that the desolvation step is still possibly the rate-determining step. The possible explanation is that the UIO-66 channel topography is straighter and more vertical to Zn electrode than that of MOF-808 (see Figure 6 and Figure 7), thus the desolvation and ion transfer is much easier in UIO-66.

4.3 Electrochemical Impedance Spectroscopy (EIS)

4.3.1. The effect of UIO-66 additive activation temperature

UIO-66 additive activated under different temperatures were added inside the Zn vs Zn coin cell battery to be tested for EIS curves. Additionally, the EIS curves under different temperatures of a single coin cell battery were also obtained. The EIS curve should be a rather perfect semicircle, which intersects the Z'(a) axis twice. The left point represents the Ohm impedance, while distance between the left and right point (the diameter of semicircle) represents the charge transfer impedance. As the testing temperature increases, the charge transfer impedance goes down, making the diameter of semicircle shorter.

As it is shown in Figure 22, it is clearly seen that the constantly-2.5 Ω Ohm impedance is neither related to temperature nor the UIO-66 additive. On the contrary, the charge transfer impedance is related to both testing temperature and the activation temperature of UIO-66 additive. In a single graph, it is noticeable that as the testing temperature increases, the charge transfer impedance decreases. If multiple graphs are compared with each other, it is noticeable that as the activation temperature of UIO-66 additive decreases, the charge transfer impedance decreases as well. The 2wt% UIO-66 additive (room) showed the best charge transfer impedance during the

test. This result is consistent with the battery test result, showing 2wt% UIO-66 additive (room) is the most successful one.

However, due to the limitation of the instrument which conducts this experiment, the semicircle is not perfect, and it does not intersect the Z'(a) axis on the right. In order to get the charge transfer impedance, here is an approximate estimation. Set Z'(b) to -20, and a straight line intersects the semicircle with two points, and their Z'(a) are marked as x_2 and x_3, respectively. Then, set Z'(b) to 0, and a straight line should ideally intersect the semicircle with two points. x_1 is known, but x_4 seems not existing. It is assumed that the semicircle could be symmetric, thus the symmetry axis should be constant. Thus, the average of x_2 and x_3 equals the average of x_1 and x_4. Then x_4 is known, and the charge transfer impedance equals the gap between x_1 and x_4

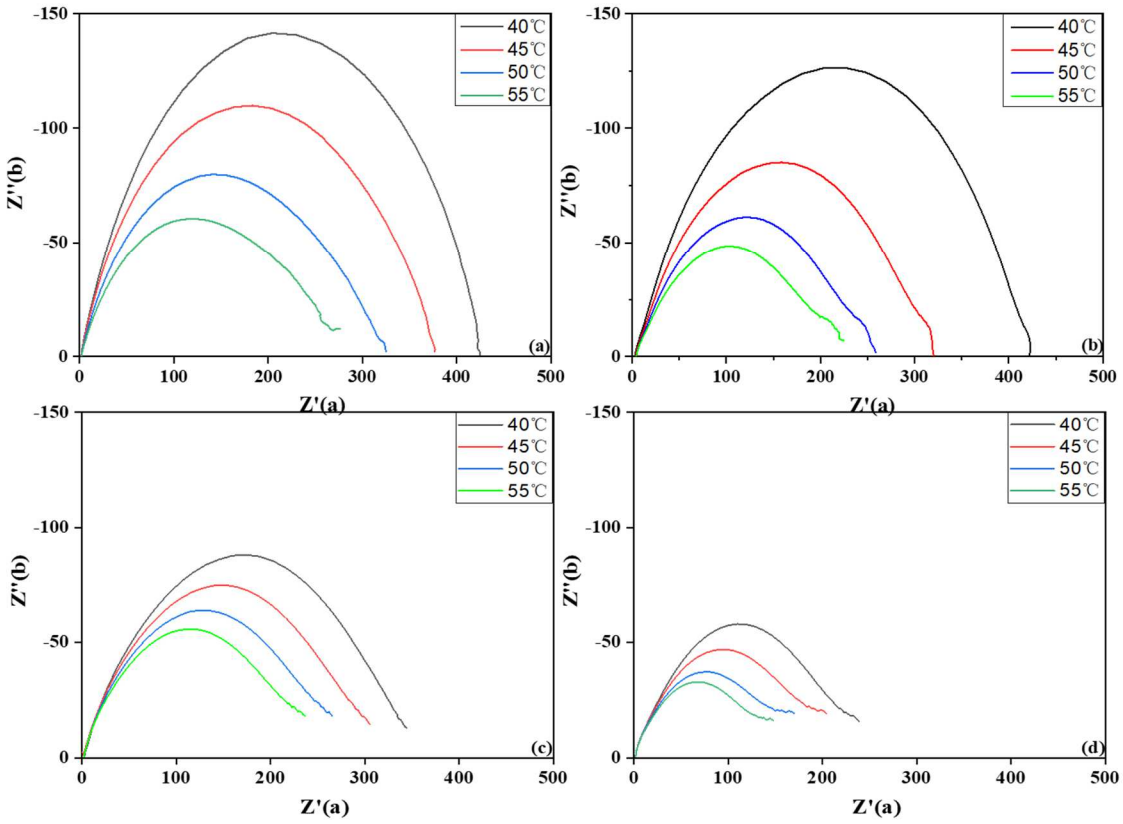

Figure 22. The comparison EIS results of Zn vs Zn symmetric battery with UIO-66 additive under different activation temperatures (a) without UIO-66 (b) 2M $ZnSO_4$ plus 2wt% UIO-66 (300C) additive (c) 2M $ZnSO_4$ plus 2wt% UIO-66 (120C) additive (d) 2M $ZnSO_4$ plus 2wt% UIO-66 (room) additive

4.3.2. The effect of MOF-808 additive activation temperature

MOF-808 additive activated under different temperatures were added inside the Zn vs Zn coin cell battery to be tested for EIS curves. As it is shown in Figure 23, it is clearly seen that the constantly-2.5 Ω Ohm impedance is neither related to temperature nor the MOF-808 additive. The overpotential turns bigger when MOF-808 were added inside, though the charge transfer

impedance decreases as the activation temperature of MOF-808 additive decreases. This is not consistent with the battery test result.

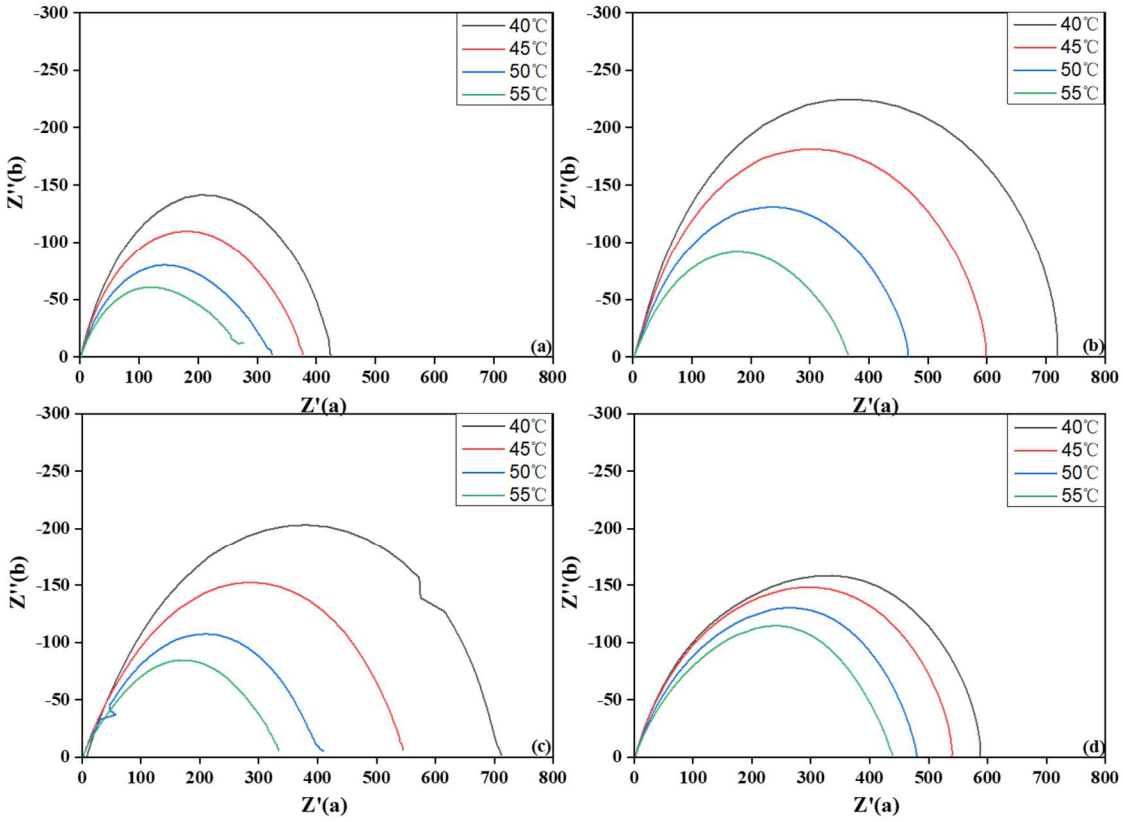

Figure 23. The comparison EIS results of Zn vs Zn symmetric battery with MOF-808 additive under different activation temperatures (a) without MOF-808 (b) 2M $ZnSO_4$ plus 2wt% MOF-808 (300C) additive (c) 2M $ZnSO_4$ plus 2wt% MOF-808 (120C) additive (d) 2M $ZnSO_4$ plus 2wt% MOF-808 (room) additive

5 Conclusion

Starting from beaker cell, pouch cell next and coin cell at last, the Zn vs Zn symmetric battery testing platform is successfully founded. Additionally, it is also found that glass fiber is the suitable separator for aqueous Zn-ion battery, while polypropylene increases the overpotential of Zn vs Zn symmetric battery and decreases the cycling life. Finally, pressure is also important for making the Zn vs Zn symmetric battery, and the most optimized pressure is 700psi for the coin cell testing platform. Larger pressure can result in the short circuit, while smaller pressure cannot fully enclose the space, which leaves a chance for electrolyte evaporation and the following bad result.

Zn vs Zn symmetric battery with the standard 2M $ZnSO_4$ cannot maintain a long cycling life which is only 150 hours, and it can only be run at a rather small constant areal current density which is 0.25 mA/cm^2. The overpotential can reach up to 150 mV and it is very unstable, representing a large resistance during charging and an unstable interface. However, Zr-based MOFs, UIO-66 and MOF-808, both show effective as they are added into standard electrolyte for Zn vs Zn symmetric battery. The overpotential can be stably decreased at least 50%, and the Zn vs Zn symmetric battery can survive when constant areal current density is up to 0.50 mA/cm^2 and 1.00 mA/cm^2

The concentration of MOFs additive seems irrelevant to decreasing the overpotential, however, high activation temperature can vanish the reversibility. The possible reason is that MOFs activated with high temperature loses the reversibility of desolvation and solvation of $[Zn(H_2O)_6]^{2+}$. For both UIO-66 and MOF-808, the overpotential and longevity are the best when

the activation temperature is lowest at 60 °C. EIS further shows that the charge transfer impedance of UIO-66 and MOF-808 are decreased as the activation temperature goes from 300 °C to 60 °C.

In general, UIO-66 gives better battery performance than MOF-808. UIO-66 (room) even amazingly shows immobile overpotential as the areal current density increases, while MOF-808 (room) only shows stable cycling life under the increasing current density. EIS also shows that the UIO-66 additive activated in different temperatures all decrease the charge transfer impedance of 2M $ZnSO_4$ standard electrolyte, while MOF-808 additive activated in different temperatures all increase the charge transfer impedance. The possible reason is that UIO-66 tunnel topography has straighter and more vertical to Zn electrode, which generates an easier pass way for $[Zn(H_2O)_6]^{2+}$ to desolvate and transfer. This paper provides a new approach and insight for developing a reversible aqueous Zn-ion battery. The Zr-based MOFs is reversible for the desolvation and solvation of $[Zn(H_2O)_6]^{2+}$ complex structure, thus decreases the overpotential and enhances the battery longevity.

6 Future work

The mechanism of how MOFs help improve the reversibility of aqueous Zn-ion battery is not surely revealed. The desolvation and solvation process need a direct and clear characterization.

Next, the testing program for getting columbic efficiency of aqueous Zn-ion battery is still under development. The evaluation must come from a reliable and reasonable testing program, and a good columbic efficiency can further prove a good reversibility due to a less severe water-splitting side reaction.

Then, the solid electrolyte interface (SEI) forming during the charge process, is also an important topic. It is related to the electrolyte content. Learning the nature of SEI and their property is vital, and this can be the instruction of modifying this interface to give a better performance of the battery.

Finally, the full cell battery Zn vs MnO_2 should be developed, as well as the mechanism of Zn^{2+} intercalation and deintercalation into MnO_2

7 References

1. Dunn, B., Kamath, H., & Tarascon, J.-M. (2011). Electrical Energy Storage for the Grid: A Battery of Choices. *Science*, *334*(6058), 928–935.

2. Konarov, A., Voronina, N., Jo, J. H., Bakenov, Z., Sun, Y.-K., & Myung, S.-T. (2018). Present and Future Perspective on Electrode Materials for Rechargeable Zinc-Ion Batteries. *ACS Energy Letters*, *3*(10), 2620–2640.

3. *Greenhouse Gas Inventory Data Explorer | US EPA*. (2020). United States Environmental Protection Agency. https://cfpub.epa.gov/ghgdata/inventoryexplorer/

4. Holland, M. (2019, December 4). *Powering The EV Revolution — Battery Packs Now at $156/kWh, 13% Lower Than 2018, Finds BNEF*. CleanTechnica. https://cleantechnica.com/2019/12/04/powering-the-ev-revolution-battery-packs-now-at-156-kwh-13-lower-than-2018-finds-bnef/

5. Electric Vehicle Sales: Facts & Figures. (2019). *Edison Electric Insitute (EEI)*. Retrieved on November 24, 2020, https://www.eei.org/issuesandpolicy/electrictransportation/Documents/FINAL_EV_Sales_Update_April2019.pdf/

6. *NPR Cookie Consent and Choices*. (2020, September 24). National Public Radio (NPR). https://choice.npr.org/index.html?origin=https://www.npr.org/2020/09/24/916625380/california-governor-on-his-order-to-ban-sale-of-new-gasoline-vehicles-by-2035

7. Wood, D. L., Li, J., & Daniel, C. (2015). Prospects for reducing the processing cost of lithium ion batteries. *Journal of Power Sources*, *275*, 234–242.

8. Yoshino, A. (2012). The Birth of the Lithium-Ion Battery. *Angewandte Chemie International Edition*, *51*(24), 5798–5800.

9. *State of the Art of Small Spacecraft Technology*. (2020). NASA. https://www.nasa.gov/smallsat-institute/sst-soa/power/

10. Guo, X., Zhou, J., Bai, C., Li, X., Fang, G., & Liang, S. (2020). Zn/MnO2 battery chemistry with dissolution-deposition mechanism. *Materials Today Energy*, *16*, 100396.

11. Bodeï, S., Manceau, A., Geoffroy, N., Baronnet, A., & Buatier, M. (2007). Formation of todorokite from vernadite in Ni-rich hemipelagic sediments. *Geochimica et Cosmochimica Acta*, *71*(23), 5698–5716.

12. Luo, J.-Y., & Xia, Y.-Y. (2007). Aqueous Lithium-ion Battery LiTi2(PO4)3/LiMn2O4 with High Power and Energy Densities as well as Superior Cycling Stability**. *Advanced Functional Materials*, *17*(18), 3877–3884.

13. Tarascon, J.-M., & Armand, M. (2001). Issues and challenges facing rechargeable lithium batteries. *Nature*, *414*(6861), 359–367.

14. Wang, J., Liao, L., Li, Y., Zhao, J., Shi, F., Yan, K., Pei, A., Chen, G., Li, G., Lu, Z., & Cui, Y. (2018). Shell-Protective Secondary Silicon Nanostructures as Pressure-Resistant High-Volumetric-Capacity Anodes for Lithium-Ion Batteries. *Nano Letters*, *18*(11), 7060–7065

15. Wang, H., Li, Y., Li, Y., Liu, Y., Lin, D., Zhu, C., Chen, G., Yang, A., Yan, K., Chen, H., Zhu, Y., Li, J., Xie, J., Xu, J., Zhang, Z., Vilá, R., Pei, A., Wang, K., & Cui, Y. (2019). Wrinkled Graphene Cages as Hosts for High-Capacity Li Metal Anodes Shown by Cryogenic Electron Microscopy. *Nano Letters*, *19*(2), 1326–1335.

16. Chan, C. K., Peng, H., Liu, G., McIlwrath, K., Zhang, X. F., Huggins, R. A., & Cui, Y. (2007). High-performance lithium battery anodes using silicon nanowires. *Nature Nanotechnology*, *3*(1), 31–35.

17. Xia, F., Kwon, S., Lee, W. W., Liu, Z., Kim, S., Song, T., Choi, K. J., Paik, U., & Park, W. I. (2015). Graphene as an Interfacial Layer for Improving Cycling Performance of Si Nanowires in Lithium-Ion Batteries. *Nano Letters*, *15*(10), 6658–6664.

18. Salvatierra, R. V., López□Silva, G. A., Jalilov, A. S., Yoon, J., Wu, G., Tsai, A., & Tour, J. M. (2018). Suppressing Li Metal Dendrites Through a Solid Li□Ion Backup Layer. *Advanced Materials*, *30*(50), 1803869.

19. Ni, J., Fu, S., Wu, C., Maier, J., Yu, Y., & Li, L. (2016). Self-Supported Nanotube Arrays of Sulfur-Doped TiO2 Enabling Ultrastable and Robust Sodium Storage. *Advanced Materials*, *28*(11), 2259–2265.

20. Chen, S., Wu, C., Shen, L., Zhu, C., Huang, Y., Xi, K., Maier, J., & Yu, Y. (2017). Challenges and Perspectives for NASICON-Type Electrode Materials for Advanced Sodium-Ion Batteries. *Advanced Materials*, *29*(48), 1700431.

21. Pramudita, J. C., Sehrawat, D., Goonetilleke, D., & Sharma, N. (2017). An Initial Review of the Status of Electrode Materials for Potassium-Ion Batteries. *Advanced Energy Materials*, *7*(24), 1602911.

22. Chao, D., Zhou, W., Xie, F., Ye, C., Li, H., Jaroniec, M., & Qiao, S.-Z. (2020). Roadmap for advanced aqueous batteries: From design of materials to applications. *Science Advances*, *6*(21), eaba4098.

23. Rajagopalan, R., Tang, Y., Jia, C., Ji, X., & Wang, H. (2020). Understanding the sodium storage mechanisms of organic electrodes in sodium ion batteries: issues and solutions. *Energy & Environmental Science*, *13*(6), 1568–1592.

24. Wang, F., Wu, X., Li, C., Zhu, Y., Fu, L., Wu, Y., & Liu, X. (2016). Nanostructured positive electrode materials for post-lithium ion batteries. *Energy & Environmental Science*, *9*(12), 3570–3611.

25. Du, W., Ang, E. H., Yang, Y., Zhang, Y., Ye, M., & Li, C. C. (2020). Challenges in the material and structural design of zinc anode towards high-performance aqueous zinc-ion batteries. *Energy & Environmental Science*, *13*(10), 3330–3360.

26. Blanc, L. E., Kundu, D., & Nazar, L. F. (2020). Scientific Challenges for the Implementation of Zn-Ion Batteries. *Joule*, *4*(4), 771–799.

27. Fang, G., Zhou, J., Pan, A., & Liang, S. (2018). Recent Advances in Aqueous Zinc-Ion Batteries. *ACS Energy Letters*, *3*(10), 2480–2501.

28. Ming, J., Guo, J., Xia, C., Wang, W., & Alshareef, H. N. (2019). Zinc-ion batteries: Materials, mechanisms, and applications. *Materials Science and Engineering: R: Reports*, *135*, 58–84.

29. Selvakumaran, D., Pan, A., Liang, S., & Cao, G. (2019). A review on recent developments and challenges of cathode materials for rechargeable aqueous Zn-ion batteries. *Journal of Materials Chemistry A*, *7*(31), 18209–18236.

30. Qiao, Y., Jiang, K., Deng, H., & Zhou, H. (2019). A high-energy-density and long-life lithium-ion battery via reversible oxide–peroxide conversion. *Nature Catalysis*, *2*(11), 1035–1044.

31. Yan, C., Li, H.-R., Chen, X., Zhang, X.-Q., Cheng, X.-B., Xu, R., Huang, J.-Q., & Zhang, Q. (2019). Regulating the Inner Helmholtz Plane for Stable Solid Electrolyte Interphase on Lithium Metal Anodes. *Journal of the American Chemical Society*, *141*(23), 9422–9429.

32. Yang, H., Chang, Z., Qiao, Y., Deng, H., Mu, X., He, P., & Zhou, H. (2020). Constructing a Super□Saturated Electrolyte Front Surface for Stable Rechargeable Aqueous Zinc Batteries. *Angewandte Chemie International Edition*, *59*(24), 9377–9381.

33. Wang, F., Borodin, O., Gao, T., Fan, X., Sun, W., Han, F., Faraone, A., Dura, J. A., Xu, K., & Wang, C. (2018). Highly reversible zinc metal anode for aqueous batteries. *Nature Materials*, *17*(6), 543–549.

34. Cao, L., Li, D., Hu, E., Xu, J., Deng, T., Ma, L., Wang, Y., Yang, X.-Q., & Wang, C. (2020). Solvation Structure Design for Aqueous Zn Metal Batteries. *Journal of the American Chemical Society*, *142*(51), 21404–21409.

35. Hao, J., Yuan, L., Ye, C., Chao, D., Davey, K., Guo, Z., & Qiao, S.□Z. (2021). Boosting Zinc Electrode Reversibility in Aqueous Electrolytes by Using Low□Cost Antisolvents. *Angewandte Chemie International Edition*, https://doi.org/10.1002/anie.202016531

36. Cataldo, F. (2015). A Revision of the Gutmann Doner Numbers of a Series of Phosphoramides including TEPA. *European Chemical Bulletin*, *2015*(42), 92–97.

37. Cao, L., Li, D., Deng, T., Li, Q., & Wang, C. (2020). Hydrophobic Organic□Electrolyte□Protected Zinc Anodes for Aqueous Zinc Batteries. *Angewandte Chemie International Edition*, *59*(43), 19292–19296.

38. Butova, V. V., Soldatov, M. A., Guda, A. A., Lomachenko, K. A., & Lamberti, C. (2016). Metal-organic frameworks: structure, properties, methods of synthesis and characterization. *Russian Chemical Reviews*, *85*(3), 280–307.

39. Furukawa, H., Gándara, F., Zhang, Y.-B., Jiang, J., Queen, W. L., Hudson, M. R., & Yaghi, O. M. (2014). Water Adsorption in Porous Metal–Organic Frameworks and Related Materials. *Journal of the American Chemical Society*, *136*(11), 4369–4381.

40. Katz, M. J., Brown, Z. J., Colón, Y. J., Siu, P. W., Scheidt, K. A., Snurr, R. Q., Hupp, J. T., & Farha, O. K. (2013). A facile synthesis of UiO-66, UiO-67 and their derivatives. *Chemical Communications*, *49*(82), 9449.

41. Wiersum, A. D., Soubeyrand-Lenoir, E., Yang, Q., Moulin, B., Guillerm, V., Yahia, M. B., Bourrelly, S., Vimont, A., Miller, S., Vagner, C., Daturi, M., Clet, G., Serre, C., Maurin, G., & Llewellyn, P. L. (2011). An Evaluation of UiO-66 for Gas-Based Applications. *Chemistry - An Asian Journal*, *6*(12), 3270–3280

42. Wang, A., Zhou, Y., Wang, Z., Chen, M., Sun, L., & Liu, X. (2016). Titanium incorporated with UiO-66(Zr)-type Metal–Organic Framework (MOF) for photocatalytic application. *RSC Advances*, *6*(5), 3671–3679.

43. Chen, X., Chen, D., Li, N., Xu, Q., Li, H., He, J., & Lu, J. (2020). Modified-MOF-808-Loaded Polyacrylonitrile Membrane for Highly Efficient, Simultaneous Emulsion Separation and Heavy Metal Ion Removal. *ACS Applied Materials & Interfaces*, *12*(35), 39227–39235.

44. Luo, H. B., Ren, Q., Wang, P., Zhang, J., Wang, L., & Ren, X. M. (2019). High Proton Conductivity Achieved by Encapsulation of Imidazole Molecules into Proton-Conducting MOF-808. *ACS Applied Materials & Interfaces*, *11*(9), 9164–9171.

45. Luo, Q. X., An, B. W., Ji, M., Park, S. E., Hao, C., & Li, Y. Q. (2014). Metal–organic frameworks HKUST-1 as porous matrix for encapsulation of basic ionic liquid catalyst: effect of chemical behaviour of ionic liquid in solvent. *Journal of Porous Materials*, *22*(1), 247–259.

46. Luo, Q. X., An, B. W., Ji, M., & Zhang, J. (2018). Hybridization of metal–organic frameworks and task-specific ionic liquids: fundamentals and challenges. *Materials Chemistry Frontiers*, *2*(2), 219–234.

47. Shen, L., Wu, H. B., Liu, F., Brosmer, J. L., Shen, G., Wang, X., Zink, J. I., Xiao, Q., Cai, M., Wang, G., Lu, Y., & Dunn, B. (2018). Creating Lithium-Ion Electrolytes with Biomimetic Ionic Channels in Metal-Organic Frameworks. *Advanced Materials*, *30*(23), 1707476.

48. Shen, L., Wu, H. B., Liu, F., Shen, J., Mo, R., Chen, G., Tan, G., Chen, J., Kong, X., Lu, X., Peng, Y., Zhu, J., Wang, G., & Lu, Y. (2020). Particulate Anion Sorbents as Electrolyte Additives for Lithium Batteries. *Advanced Functional Materials*, *30*(49), 2003055.

49. Lu, X., Wu, H., Kong, D., Li, X., Shen, L., & Lu, Y. (2020). Facilitating Lithium-Ion Conduction in Gel Polymer Electrolyte by Metal-Organic Frameworks. *ACS Materials Letters*, *2*(11), 1435–1441.

50. Hon Lau, C., Babarao, R., & Hill, M. R. (2013). A route to drastic increase of CO_2 uptake in Zr metal organic framework UiO-66. *Chemical Communications*, *49*(35), 3634.